

Supporting Information for

N-doped Graphene Frameworks with Superhigh Surface Area: Excellent Electrocatalytic Performance for Oxygen Reduction

Huijuan Cui,^{a,b} Hongmei Yu,^c Jianfeng Zheng,^{*a} Zhijian Wang,^a Yanyan Zhu,^{a,b} Suping Jia,^a Jia Jia,^c and Zhenping Zhu^{*a}

^aState Key Laboratory of Coal Conversion, Institute of Coal Chemistry, Chinese Academy of Sciences, Taiyuan, 030001, China, ^b University of Chinese Academy of Sciences, Beijing, 100049, China, ^c Fuel Cell System and Engineering Laboratory, Dalian Institute of Chemical Physics, Chinese Academy of Sciences, 457 Zhongshan Road, Dalian 116023, China.

Address correspondence to zpzhu@sxicc.ac.cn; zhengjf@sxicc.ac.cn

This supplementary information containing
The fabricated method of fuel cell
Figures S1-S13
References 1-2

The fabricated method of fuel cell

The single cell was fabricated using the as-prepared NGFs as the cathode (0.5 mg/cm²) and 70% Pt/C as the anode (0.5 mg/cm²). The area of the single cell was 0.5 cm². Besides, the AEH9620 membrane and a home-made resin were used to assemble the cell. During the performance test, the cell operating temperature was 50 °C. Then, H₂ and O₂ (99.99% pure) with corresponding flow rates of 100 and 200 sccm at 0.1 MPa (backpressure) were fed into the anode and the cathode, respectively. Both gases were humidified through a humidifier at the operating temperature before feeding into a single cell. To make a comparison, the cell using Pt/C catalyst (20%) as the cathode was also fabricated with the same method.

Figures S1-S13

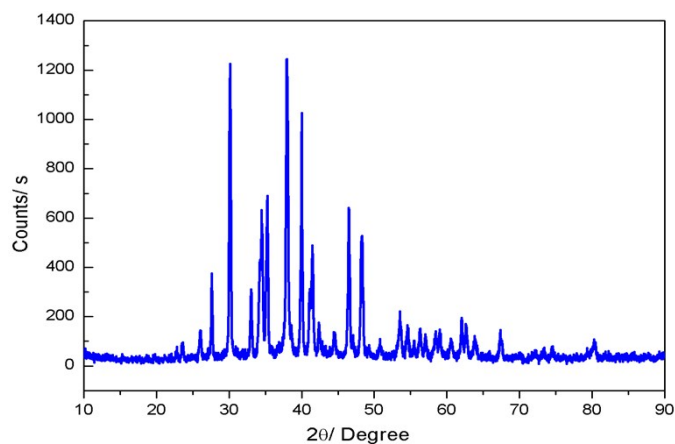


Figure S1. XRD pattern of fast pyrolysis product before purification. As shown in the Experimental Section, the NGFs were synthesized by fast pyrolysis of mixture of glycine and sodium carbonate. As the process was fast, typically two minutes, the Na_2CO_3 particles did not be decomposed. The sodium-containing material after fast pyrolysis process is still Na_2CO_3 , (PDF:37-0451), without the signal of other sodium-containing materials.

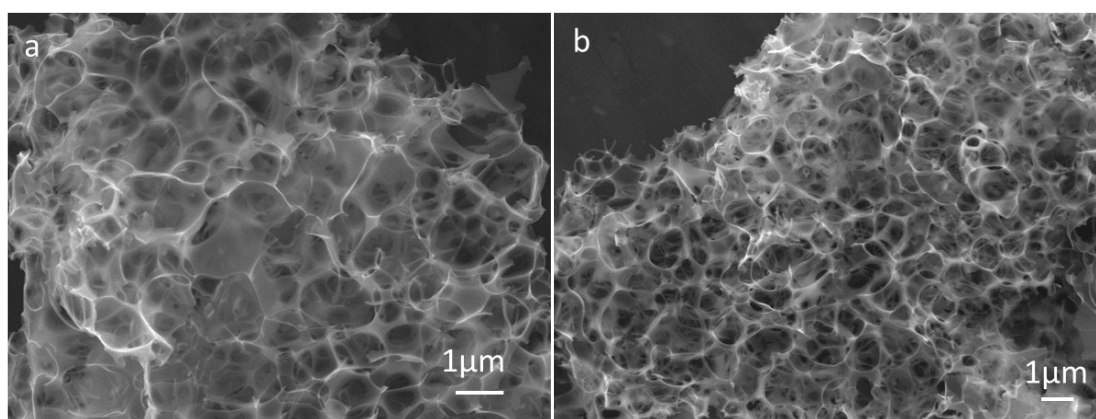


Figure S2. SEM image of the N-doped graphene synthesized from a fast pyrolysis at (a) 800 °C (NGFs-800) and (b) 900 °C (NGFs-900). Both of them show a well-organized framework structure.

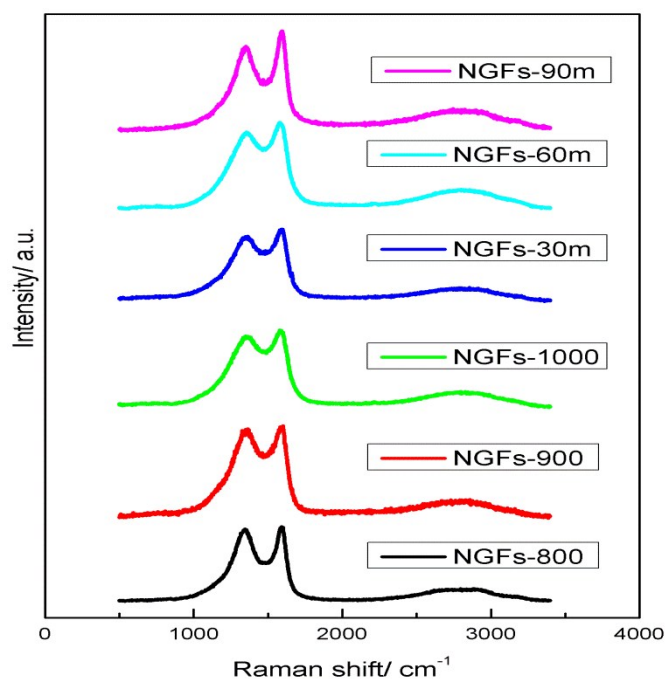


Figure S3. Raman spectra of the NGFs samples. The bands at 1360 cm^{-1} , 1590 cm^{-1} and 2750 cm^{-1} are corresponding to the D, G and 2D bands, respectively.¹

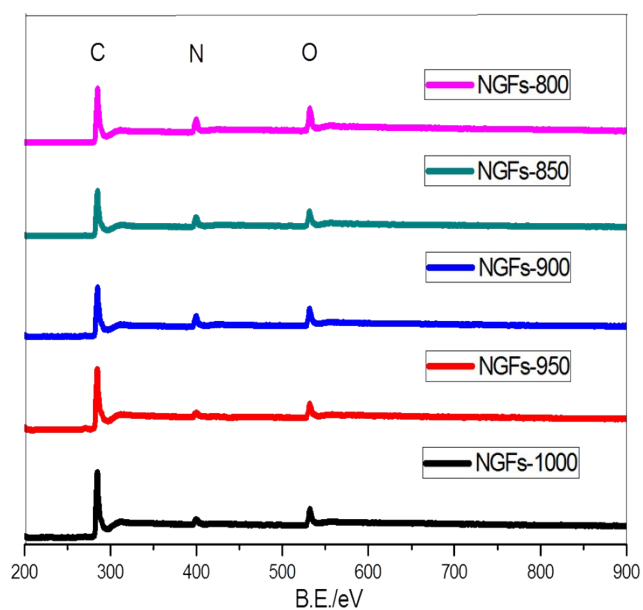


Figure S4. XPS survey spectra of the NGFs samples synthesized at different temperatures. The peak at 284 eV , 400 eV and 532 eV are C, N and O, respectively.

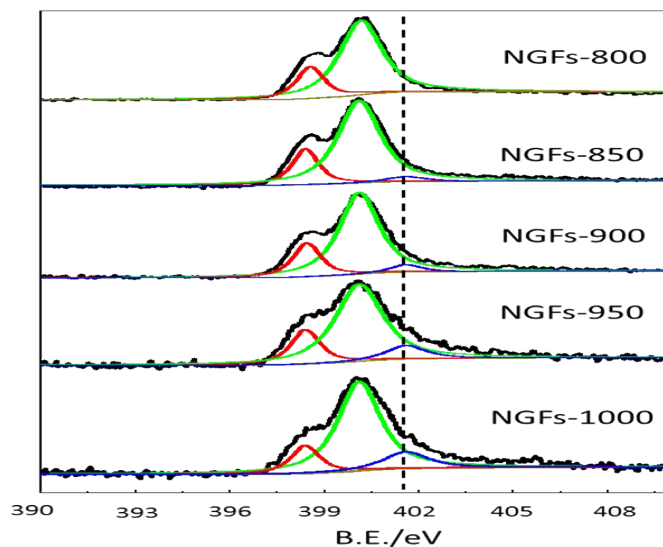


Figure S5. N1s XPS spectra for the NGFs synthesized at different temperatures. The three fitted peaks are pyridinic-N at 398.4 eV (red), pyrrolic-N at 400 eV (green), and graphitic-N at 401.6 eV (blue).² Obviously, pyrrolic-N is dominant in the as-synthesized samples, while graphitic-N increases in content with increasing pyrolysis temperature.

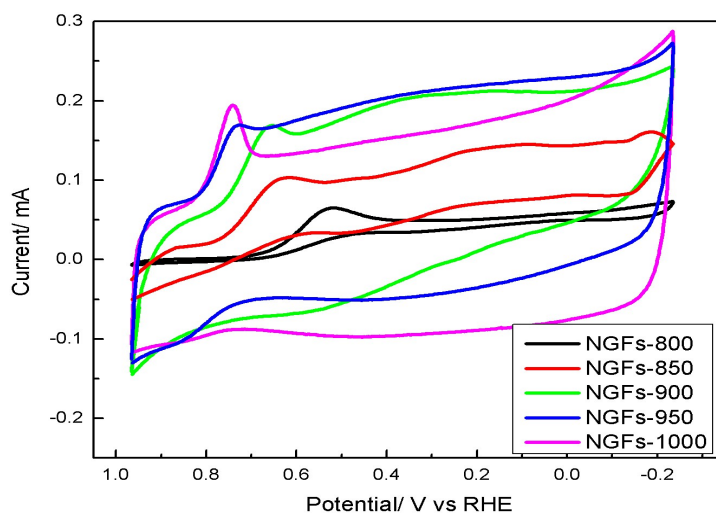


Figure S6. CV curves of ORR on the electrodes modified with the NGFs synthesized at different temperatures in O₂-saturated 0.1 M KOH at a scan rate of 10 mV/s. Obviously, with increasing pyrolysis temperature, the reduction peak shifts to less negative potential and the peak current became larger.

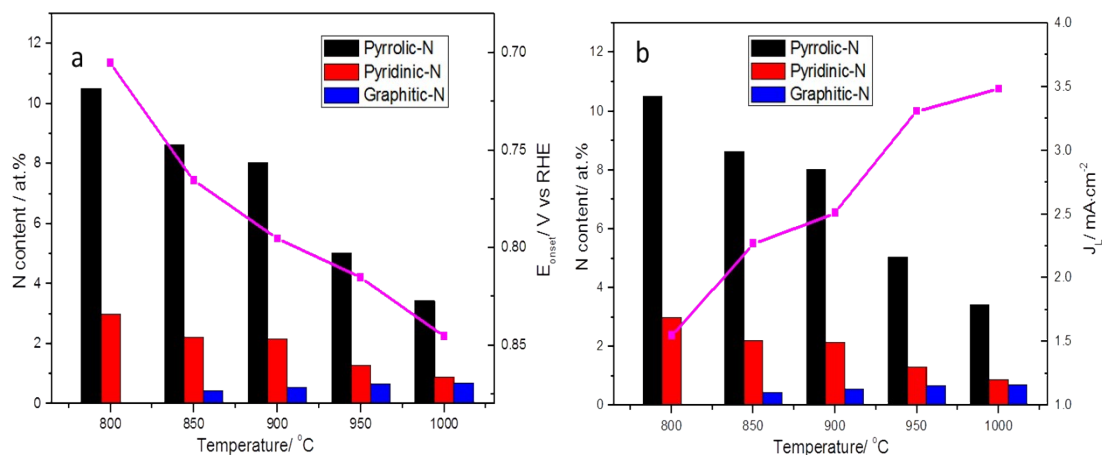


Figure S7. The relevancy of E_{onset} and J_L to the absolute content (atomic percent in carbon) of different C-N configuration.

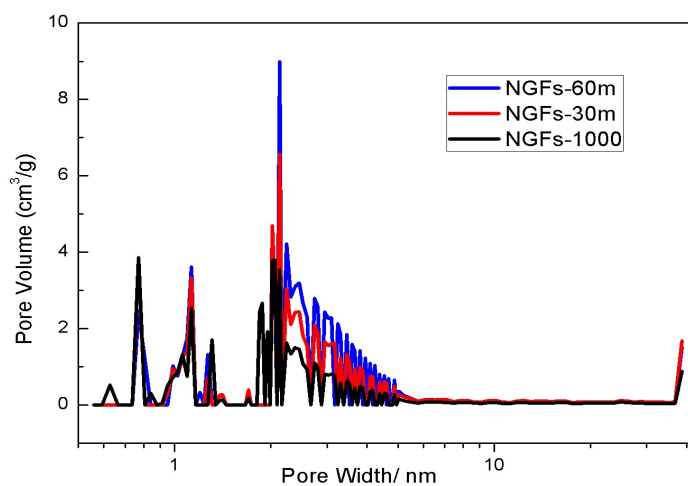


Figure S8. The pore distribution of the three NGFs. The pore distribution of the three NGFs were similar, with the pore width of 0.5~5 nm. The meso- and nano-porosity led to the large specific surface area. In addition, after annealing at 1000°C, the pore distribution at 2~5 nm increased, which may be produced by the significant loss of oxygen and nitrogen atoms induced by thermal modulation. This process would create predictably porous vacancies in graphene network and enlarge graphene edge, which led to the increase of specific surface area.

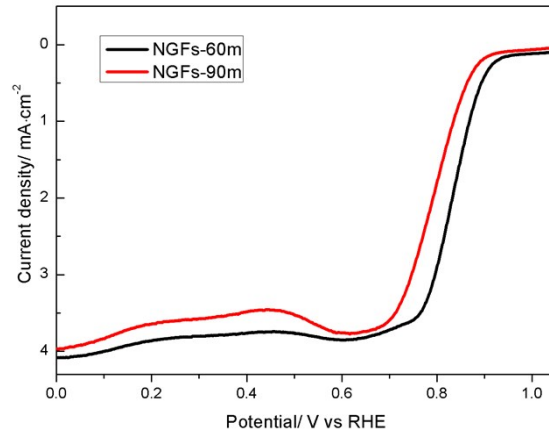


Figure S9. LSV curves of NGFs-60m and NGFs-90m.

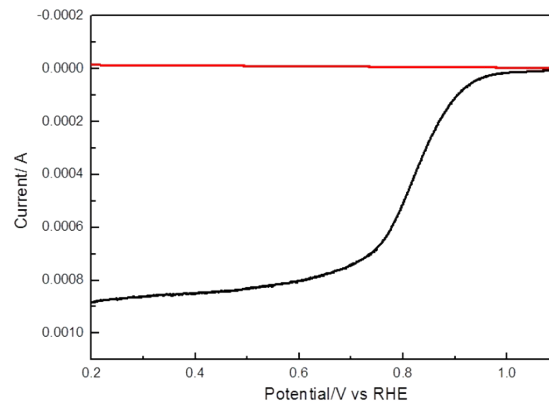


Figure S10. LSV curve on Pt/C-modified RRDE. The calculated value of n is 3.9, indicating a good 4e pathway for ORR.

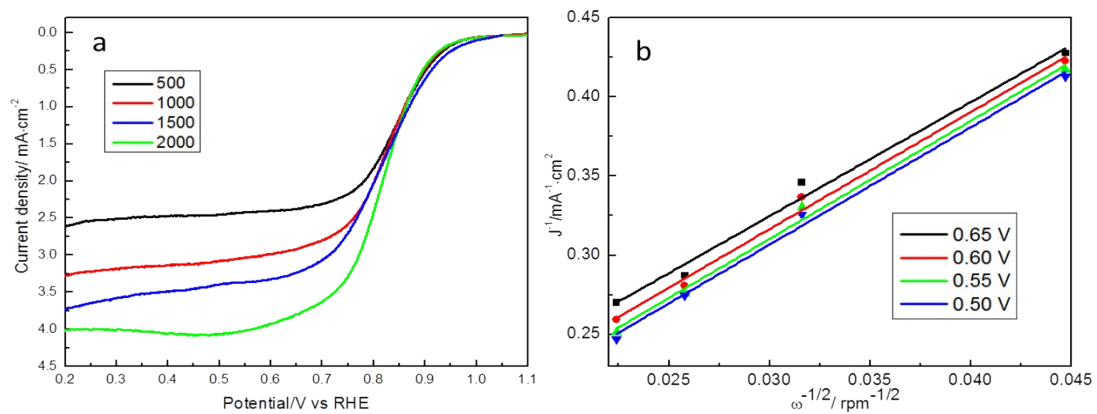


Figure S11. a, LSV curves of ORR for Pt/C-modified RDE at different rotation rates.

b, Koutecky–Levich plots obtained from the LSV curves in **a**.

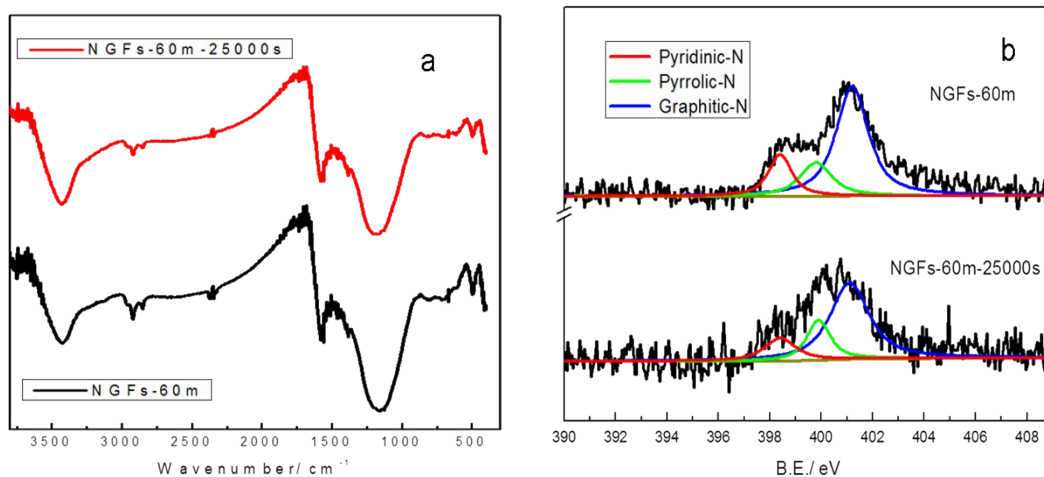


Figure S12. FT-IR (a) and XPS (b) spectrum of NGFs-60m and NGFs-60m-25000s.

The C-N structures of NGFs before and after 25000s were further characterized by XPS and FT-IR. As shown in Figure S12a, the FT-IR spectrum of NGFs-60m was almost the same as NGFs-60m-25000s, which suggest that there were few changes produced before and after stability test. This result was consistent with the XPS analysis (Figure S12b). The graphitic-N was still dominant in NGFs-60m-25000s and the relevant content of graphitic-N, pyridinic-N and pyrrolic-N were 63.5%, 16.0% and 20.5%, which were nearly the same as these in NGFs-60m. These results suggest the good structure stability of NGFs-60m. The unchanged onset potential before and after stability test should be due to the stable C-N active sites.

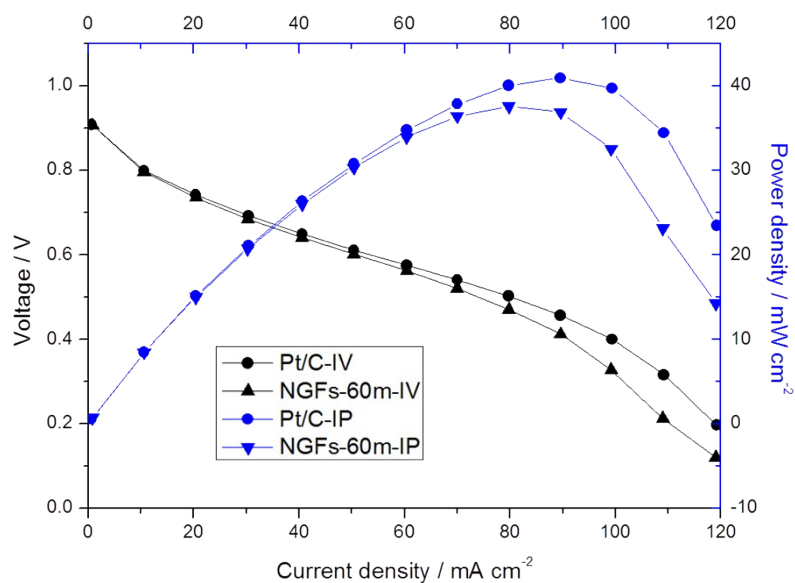


Figure S13. The I-V and I-P curves of the two cells.

The open circuit voltage of NGFs-60m-modified cell was almost the same as Pt/C-modified cell, indicating the high catalytic activity of C-N sites. However, the maximum power density of NGFs-60m-modified cell was 38 mW/ cm², which was a little lower than the Pt/C-modified cell (41 mW/ cm²). It may be due to the thicker film of NGFs-60m-modified cathode or the weaker wettability between NGFs-60m and the home-made resin.³ Owing to the lower density of NGFs-60m, the film of NGFs-60m-modified cathode would be thicker than Pt/C-modified cathode, which should be unfavorable for the transport of the home-made resin. And therefore, it could lead to a little poorer cell performance of NGFs-60m. Besides, the weaker wettability between NGFs-60m and the home-made resin can also cause the loss of cell performance. The cell performance of NGFs-60m may be improved by optimizing the experiment conditions such as the type of resin and the dosage of resin, which should be studied in the future.

Table S1. The results of NGFs based on the elemental analysis.

Samples	N	C	O	H	N/C ^a	N/C ^b
	(wt.%)	(wt.%)	(wt.%)	(wt.%)	(at.)	(at.)
NGFs-800	13.77	60.65	22.47	3.11	0.19	0.19
NGFs-900	11.79	62.58	22.84	2.79	0.16	0.14
NGFs-1000	8.77	72.83	15.85	2.55	0.10	0.06
NGFs-15m	5.87	84.01	8.45	1.67	0.06	0.04
NGFs-30m	4.91	86.1	7.74	1.25	0.04	0.02
NGFs-60m	2.93	90.88	5.16	1.03	0.03	0.02

Note: a, N/C atom percentage obtained by element analysis. b, N/C atom percentage obtained by XPS analysis.

The elemental analysis was used to detect the N content of NGFs. As shown in Table S1, the nitrogen content of NGFs samples were decreased with the increase of pyrolysis temperature and time. The weight percent of N in NGFs-800 was 13.77%, which was decreased to 8.77% with the pyrolysis temperature increased to 1000 °C. After thermal annealing of NGFs-1000 for 60 min, the weight percent of N was turned to 2.93%. To compare the results with the XPS data, the N/C atom percentage was extracted. As shown in Table S1, the N/C atom percentages were almost similar in both elemental analysis and XPS results.

Table S2. The I_G/I_D value of NGFs samples.

	NGFs-800	NGFs-900	NGFs-1000	NGFs-30m	NGFs-60m	NGFs-90m
I_G/I_D	1.04	1.05	1.07	1.09	1.10	1.14

References

1. A. C. Ferrari, D. M. Basko, *Nat. Nanotechnol.* 2013, **8**, 235.
2. H. Gao, L. Song, W. Guo, L. Huang, D. Yang, F. Wang, Y. Zuo, X. Fan, Z. Liu, W. Gao, R. Vajtai, K. P. Hackenberg, M. Ajayan, *Carbon* 2012, **50**, 4476.
3. C. V. Rao, Y. Ishikawa, *J. Phys. Chem. C*, 2012, **116**, 4340.